ISSN 0036-0295, Russian Metallurgy (Metally), Vol. 2023, No. 13, pp. 2270–2274. © Pleiades Publishing, Ltd., 2023.
Russian Text © The Author(s), 2023, published in Tekhnologiya Metallov, 2023, No. 5, pp. 26–32.

POWDER METALLURGY TECHNOLOGIES. ADDITIVE TECHNOLOGIES

Structure Formation in 09G2S Steel Produced by Additive Electric Arc Growth

M. S. Anosov[a], *, D. A. Shatagin[a], D. A. Ryabov[a], and A. M. Mikhailov[a]

[a] *Alekseev State Technical University, Nizhny Novgorod, 603950 Russia*

**e-mail: anosov-maksim@list.ru*

Received November 15, 2022; revised December 28, 2022; accepted February 8, 2023

Abstract—Currently, additive technologies, in particular, electric arc growth as the most universal and productive, are used to produce individual machine parts. The problem of studying the process of structure formation in alloys during electric arc additive growth to ensure the necessary parameters of the microstructure of a material and its mechanical properties is challenging. 09G2S steel samples for research are fabricated on a developed test bench implementing the technology of 3D printing by electric arc surfacing, microstructural studies on an optical microscope are used, and microhardness measurements are carried out. The features of structure formation in a 09G2S alloy during additive electric arc growth have been determined, and controlled parameters have been identified to ensure the necessary parameters of the structure and, consequently, the mechanical properties of the alloy. The heat input of the surfacing process and the temperature of a thermal cycle are found to play a significant role in the structure formation in the material. The conducted research and established dependences make it possible to control the structural state of 09G2S steel during cladding to ensure the required parameters of its microstructure and mechanical properties.

Keywords: structure formation, 09G2S steel, additive technologies, electric arc cladding, cladding heat input, thermal cycle

DOI: 10.1134/S0036029523700490

INTRODUCTION

Additive technologies, namely, 3D printing with metals, have been intensively developing over the past two decades. The methods of selective laser melting (SLM) of powders, laser cladding of powder and electric arc cladding of wire are widely spread [1, 2]. Among the aforementioned methods, wire arc additive manufacturing (WAAM) [3–7] has numerous advantages, namely, high productivity (up to 12 kg/h) and uniformity. Such production technology of metal items can be successfully implemented in the existing production complexes, including CNC machines.

The operation of structures, which work for a long time in the Arctic and Far North, is necessarily associated with the need to control the physical and mechanical characteristics of the material used during the entire life cycle of products. The use of metallic materials at low temperatures is usually accompanied by a drop in impact toughness [8], and the risk of brittle fracture increases many times.

The ability of metallic materials to resist the action of dynamic loads is known to be related to the size of structural fragments (grains) [9]. In this regard, it is necessary to establish a interrelation between the technological parameters of the WAAM process and the resulting structure and properties of the material, in particular, providing the required cold resistance.

The heat input during 3D printing, thermal interlayer cycles, build rate and protective environment should be taken as controlled WAAM parameters. The proposed parameters are necessary for the creation of modern systems for controlling the structure and quality of the produced materials.

Thus, the purpose of this work is to investigate the peculiarities of structure formation in a 09G2S alloy during additive electric arc growth, as well as to determine the parameters of 3D printing necessary to form the required structure and, consequently, the mechanical properties of the alloy.

EXPERIMENTAL

A widely used 09G2S steel, which is used for welded structures that can be operated at low temperatures (down to –40°C), was chosen as the material for the research (the chemical composition is given in Table 1). The material for research was fabricated using the WAAM method (0.8 mm wire) integrated into a CNC machine. The construction of the workpiece was carried out in a CO_2 environment as a protective gas.

Table 1. Chemical composition of steel, wt %

Material	C	Si	Mn	Ni	S	P	Cr	Cu	Fe
09G2S	0.09	0.9	1.9	0.12	0.008	0.12	0.14	0.09	For balance

Voltage U, current I, wire feed speed V, gap between wire and cladded workpiece z, as well as CO_2 flow rate were taken as variable parameters of the WAAM process. The gap z, feed speed V, and shielding gas flow rate were chosen as constant variables in the experiment. In this case, $z = 11$ mm, and $V = 350$ mm/min.

During the experiment, the energy Q required for deposition of a unit weld length was determined,

$$Q = \frac{0.8IU}{V},$$

where 0.8 is the coefficient of energy loss (State Standard GOST R ISO 857-1–2009). The rest bench used for research allows changing the Q parameter in the range of 150–1200 J/mm.

The samples were made according to the following sequence: printing a layer, stopping the process and cooling the workpiece to the required temperature, printing the next layer. Thus, 3D printing was performed under three thermal cycles T_c: complete cooling of the layer (below 50°C), layer temperature 350°C according to the recommendations [11], and layer temperature 850–900°C (above the Ac_3 point). The schematic view of the influence of thermal effects from laying subsequent layers during 3D printing on a point in the workpiece is illustrated in Fig. 1.

Samples for studying the microstructure in different zones of the workpiece were cut out from three sections (next to the substrate, in the central part and in the final upper layers). To identify the microstructure of the material under study, short term etching in a 4% aqueous solution of nitric acid was used. The structures were imaged using a KYENCE–VHX1000 metallographic optical microscope.

The average grain size in the structures of 09G2S steel was assessed according to State Standard GOST 5639–82. To evaluate the cold resistance of the resulting material, Charpy type samples were made, which were cut from the walls along and across the cladded layers. This is due to the fact that materials made by WAAM 3D printing are characterized by anisotropy of properties [10].

Then the samples were tested on a MK-30A pendulum machine to determine impact toughness according to State Standard GOST 9454–78 at reduced temperatures (–80…+20°C) [11, 12]. The developed cryochamber [13] was used for low temperature tests.

RESULTS AND DISCUSSION

Analysis of microstructures (Fig. 2) of 09G2S steel formed at different energy modes of WAAM technology shows that the size of ferrite grains and structural homogeneity largely depend on the heat input to the cladding process. Experimentally it was determined that the most acceptable from the point of view of quality of the formed structure (the finest grain size with greater homogeneity, the smallest value of anisotropy of properties) is the structure with the mode of the heat input Q, equal to 425 J/mm. It also should be mentioned that structural macro-defects in the form of pores were detected at the heat input Q less than 190 J/mm.

Average grain sizes d formed at different energy modes of the structures of the investigated material were measured. The results obtained in [14] show a linear relationship between the heat input Q and the resulting average grain size d, which allows us to predict the structural state and properties of the formed material in the course of WAAM. Similar dependences were obtained by researchers earlier when analyzing grain sizes after welding of 09G2S steel [15].

Due to the fact that the best mechanical properties are possessed by metals and alloys with minimum grain size, including impact toughness [16, 17], the study of the thermal cycle of the WAAM process was carried out at energy $Q = 425$ J/mm.

In the general case, during 3D printing, the subsequent layer melts part of the previous layer, and not the molten metal located below undergoes recrystallization (normalization), thus, the structure of the printed workpiece made of 09G2S steel in the first layer should be represented by columnar grains, as in the weld, this is followed by a wide zone passing through

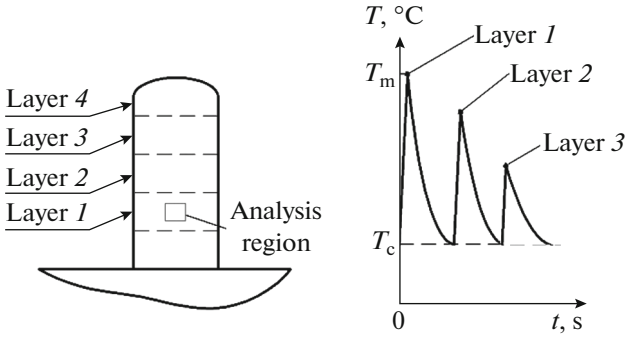

Fig. 1. Schematic view of thermal action from formation of subsequent layers on the region to be analyzed.

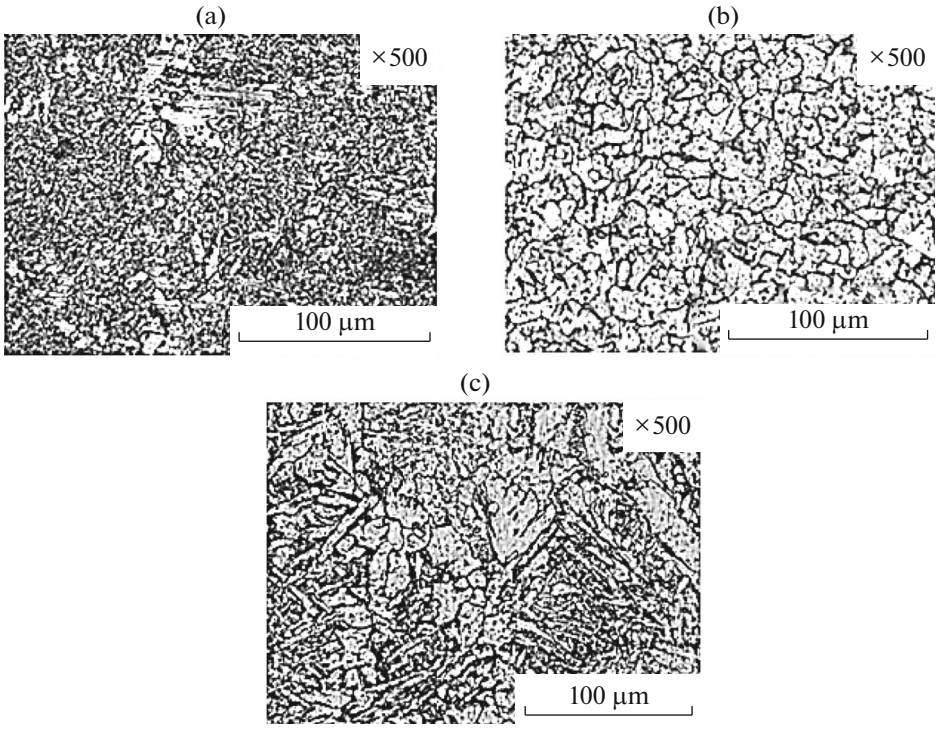

Fig. 2. Structure of 09G2S steel fabricated at an applied energy of (a) 190 (b) 425, and (c) 475 J/mm.

all layers and represented by a structure characteristic of steel after normalization, and an upper layer with an overheating zone from the welding arc, also characteristic of a conventional weld.

Next, the influence of the thermal cycle (T_c) on the microstructure and microhardness of the material under study was considered. Below are the modes of thermal cycles of cladding of 50°C (Fig. 3), 350°C (Fig. 4), and 850–900°C (Fig. 5).

Figure 3 shows that the sample formed by printing on cooled metal has three characteristic zones. The first layer contains fine grains of ferrite, oriented in the direction of heat removal; the upper layer is represented by an overheating zone with signs of dendrites. Predominantly, including the central part, the sample consists of ferrite and pearlite grains normalized by the cyclic thermal effects of the printing process, the average grain size of ferrite is 15 μm. The structure has a

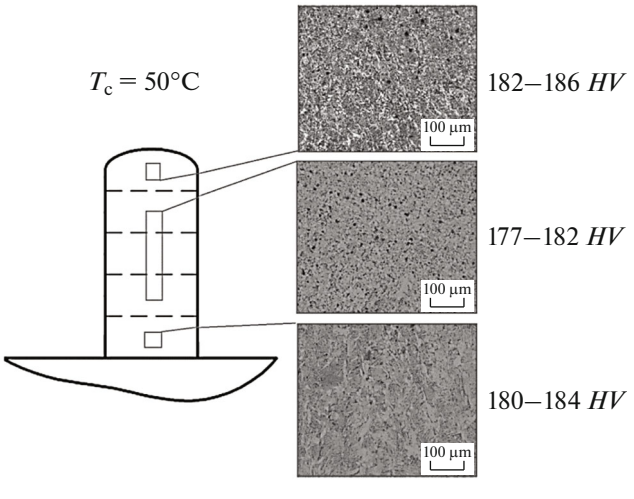

Fig. 3. Results of microstructural investigations and estimation of *HV* microhardness along the height of the clad wall at a thermal cladding cycle of about 50°C.

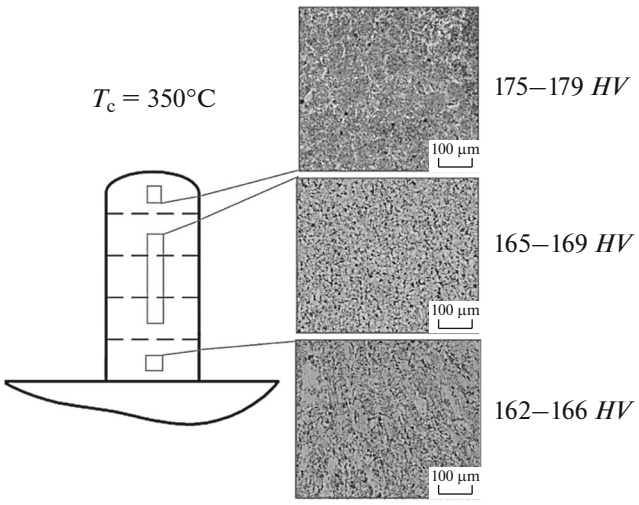

Fig. 4. Results of microstructural investigations and estimation of *HV* microhardness along the height of the clad wall at a thermal cladding cycle of about 350°C.

large number of defects in the form of pores and slag inclusions of about 6 μm in size. Evaluation of microhardness over the entire height of the clad wall shows a stable hardness between 177 and 186 *HV*.

The sample fabricated at a layer temperature of 350°C (see Fig. 4) is identical in structure to the sample produced with significant cooling (see Fig. 3). In this case, the ferrite grain size in the central part is larger and amounts to 20 μm. This is due to the fact that the entire sample received heat from the 3D printing process and was heated to 350°C, which led to an increase in the size of the overheating zone, resulting in a slight increase in grain size. Evaluation of microhardness based on the height of the deposited wall also shows a stable hardness of the middle part of the wall ranging from 165 to 169 *HV* and a higher hardness of the upper part (last layer) up to 179 *HV*. Moreover, the microhardness of the entire wall is lower than the microhardness of the wall obtained at $T_c = 50$°C.

The structure of the sample presented in Fig. 5, which formed in the course of a thermal cycle during which the temperature of the formed part of the workpiece was above 850–900°C (above Ac_3), shows that the entire sample except the first layer has signs of dendrites and overheating. The structure mainly consists of coarse ferrite grains with a size of 40–60 μm, oriented in the direction of heat removal. The first layer also has coarse grains, but does not show signs of overheating; this is due to a different heat dissipation compared to subsequent layers, because the formation of the first layer was carried out on a substrate with a temperature of 20°C. Evaluation of microhardness based on the height of the deposited wall shows a stable hardness of the middle part of the wall ranging from 142 to 150 *HV* and an increased hardness of the upper part (last layer) up to 159 *HV*. Thus, to relieve internal stresses after cladding, heat treatment should be carried out. The data obtained also correlate with the results of studies of the heat affected zone during welding of 09G2S steel [18].

A cycle of about 350°C was chosen as the optimum thermal cycle for cladding, because samples printed when the layer had completely cooled had a large number of defects in the form of pores and slag inclusions, and samples produced at temperatures above 850–900°C had a coarse grained structure and signs of overheating.

Low temperature impact tests were carried out on samples [19] obtained using various printing modes and differing in the average grain size. The results are presented in [14]. It has been established that lowering the test temperature to –40°C, near which a ductile brittle transition (T_{50}) is observed, has a significant effect on the impact toughness of the samples, reducing the values by up to two times. Thus, the operation of structures made of the metal under study at temperatures below –40°C significantly increases the likelihood of brittle fracture. The impact toughness of the printed samples was shown to be linearly related to the average grain size, a decrease in which significantly increases the resistance against loads at both positive and negative temperatures.

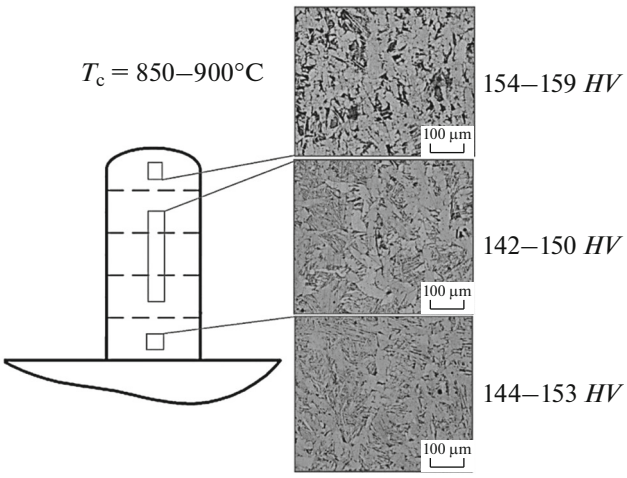

Fig. 5. Results of microstructural investigations and estimation of *HV* microhardness along the height of the clad wall at a thermal cladding cycle of about 850–900°C.

The obtained dependences of impact toughness on grain size confirm their relationship and are similar to the results of previous studies [15, 16].

CONCLUSIONS

(1) As a recommended printing mode, it is necessary to choose a mode that ensures a minimum grain size, which increases the impact toughness. The absence of macrodefects in the structure of a metal is a necessary condition.

(2) The experimental conditions at a cladding energy Q = 425 J/mm and thermal cycle of about 350°C were shown to be optimal from the point of view of forming a fine-grained structure with the minimum number of defects.

(3) The results obtained allow us to apply WAAM parts on real technical objects using the chosen printing conditions.

FUNDING

This work was supported by the Russian Science Foundation, project no. 22-79-00095 "Development of scientific and technological backgrounds of structure formation of engineering materials produced by additive electric arc growth in order to generate mechanical properties upon fatigue using artificial intelligence approaches."

CONFLICT OF INTEREST

The authors of this work declare that they have no conflicts of interest.

REFERENCES

1. A. Malladi and S.B.S. Sarma, "3D metal printing technologies," The IUP J. Mech. Eng. **X** (1), 48–54 (2017).
2. I. V. Shishkovsky, *Laser Synthesis of Functional Mesostructures and 3D Items*, (Moscow, FIZMATLIT, 2009).
3. F. Montevecchi, G. Venturini, A. Scippa, G. Campatelli, "Finite element modeling of wire-arc-additive manufacturing process," Procedia CIRP, **55**, 109–114 (2016). https://doi.org/10.1016/j.procir.2016.08.024
4. S. Williams, M. Filomeno, A. Adrian, D. Jialuo, G. Pardal, and P. Colegrove, "Wire Arc Additive Manufacturing," Mater. Sci. Technol. (2015). https://doi.org/1743284715Y.000.10.1179/1743284715Y.0000000073
5. M. A. Jackson, A. Van Asten, J. D. Morrow, S. Min, and F. E. Pfefferkorn, "Energy consumption model for additive-subtractive manufacturing processes with case study," Int. J. Prec. Eng. Manufact.-Green Technol., No. 5(4), 459–466 (2018). https://doi.org/10.1007/s40684-018-0049-y
6. J. E. Pinto-Lopera et al., "Real-time measurement of width and height of weld beads in GMAW processes," Sensors **16** (9), 1500 (2016). https://doi.org/10.3390/s16091500
7. J. Zh. Li, M. R. Alkahari, and N. A. Rosli, "Review of wire arc additive manufacturing for 3D metal printing," Int. J. Automat. Technol. (2019). https://doi.org/10.20965/ijat.2019.p0346.140.13.346-353
8. A. A. Khlybov et al., "The effect of low temperatures on the operability of products 20GL steel," J. Phys.: Conf. Ser. **1431**, 012063 (2020). https://doi.org/10.1088/1742-6596/1431/1/012063
9. V. N. Shakhov and V. V. Bogdanov, "Evaluation of grain score by fractal analysis," Aktual. Probl. Aviats. Kosmonavt., No. 10 (2014). https://cyberleninka.ru/article/n/otsenka-balla-zerna-metodom-fraktalnogo-analiza. Cited July 27, 2021.
10. Yu. G. Kabaldin, D. A. Shatagin, M. S. Anosov, P. V. Kolchin, and A.V. Kiselev, "Diagnostics of 3D-printing on a CNC machine by machine learning," Russian Eng. Res. **41** (4), 320–324 (2021).
11. *Directive RD 153–34.1–003–01. Welding, Heat Treatment and Control of Pipe Systems of Boilers and Pipelines during Installation and Repair of Power Equipment (PTM-1c). Introduction 2001-07-02* (2002).
12. Yu. G. Kabaldin, M. S. Anosov, and D. A. Shatagin, "Evaluation of the mechanism of the destruction of metals based on approaches of artificial intelligence and fractal analysis," IOP Conf. Series: Mater. Sci. Eng., **709**, 033076 (2020). https://doi.org/10.1088/1757-899X/709/3/033076
13. A. A. Khlybov, Yu. G. Kabaldin, M. S. Anosov, D. A. Ryabov, and V. I. Sentyureva, "Problems of ensuring safe operation of freight car bogies at subzero temperatures," Vestnik IzhGTU, **22** (4), 18–26 (2019). https://doi.org/10.22213/2413-1172-2019-4-18-26
14. Yu. G. Kabaldin, M. S. Anosov, D. A. Ryabov, P. V. Kolchin, D. A. Shatagin, and A. V. Kiselev, "Research of influence of 3D-printing modes on structure and cold resistance of 08G2S steel," Vestnik of Magnitogorsk Gos. Tekh. Univ. **19** (4), 64–70 (2021). https://doi.org/10.18503/1995-2732-2021-19-4-64-70
15. Yu. V. Poletaev and V. Yu. Poletaev, "Single-pass electric arc welding under thin slag layer of 09G2S steel plate structures," Vetsnik Don. Gos. Tekh. Univ. **18** (1), 50–58 (2018).
16. I. G. Uzlov, A. I. Babchenko, Zh. A. Dementieva, A. A. Kononenko, and A. L. Safronov, "Influence of wheel steel microstructure parameters on its ductile properties" in *Fundamental and Applied Issues of Ferrous Metallurgy* (Dnepropetrovsk, 2007), Vol. 14, pp. 202–210.
17. G. V. Toporov and G. Ya. Smokotin, "Influence of grain size on the impact-fatigue resistance of steel 45," Izv. Tomsk Politekh. Inst. **106**, 153–164 (1958).
18. E. Maksimova, "Study of the structure of the 09G2S grade steel welded joints performed by welding at subzero temperatures," Procedia Structural Integrity **20**, 174–179 (2019). https://doi.org/10.1016/j.prostr.2019.12.135

Translated by I. Moshkin